Frustrated Total Internal Reflection

Producing Evanescent Fields with Microwaves

Henry J. Nelson

Grinnell College, Department of Physics

May 19, 2017

Abstract

Frustrated total internal reflection with microwaves is used to produce evanescent fields between two wax prisms. The transmission across the prism gap and the reflection from gap are measured as a function of the distance between prisms and compared with theoretical predictions. Oscillatory features not predicted by theory appear in the experimental data and are investigated further. The source of these oscillations could not be confirmed but is thought to be a product of the experimental setup which was proven to exhibit effects different from those accounted for in the theory.

1 Introduction

One of the most common ways of exploring the wave nature of light is showing refraction as light changes media. This refraction at interfaces in media is famously governed by Snell's law which, because $|\sin\theta| \leq 1$ for all $\theta \in \mathbb{R}$, cannot be satisfied for some angles of incidence when the index of refraction decreases across the boundary. In these cases there is no refracted ray and total internal reflection occurs. But while the wave does not propagate across the boundary, due to the boundary conditions from Maxwell's equations, there must be non-zero electric and magnetic fields extending past the boundary into the second medium. These fields are called evanescent fields and they quickly decay to zero (exponential decay) as one moves away from the boundary in the new medium.

Even though these fields are decaying, they can still excite a new propagating wave if they reach an adequate medium. For example, if something with the same index as the original medium is encountered during the exponential decay a new propagating wave is formed. This is called Frustrated Total Internal Reflection (FTIR). Since the entire wave had previously been reflected, due to conservation of energy this newly created wave must diminish the reflected beam accordingly. This process is exactly analogous to that of tunnelling through a potential barrier in quantum mechanics, where the wave function decays exponentially in the disallowed region of high potential but then regains its wave nature on the other side.

The phenomena of evanescent fields has drawn attention from many due to its counter intuitive nature. The setup of using two right triangle prisms with total internal reflection as described in this introduction is one of the easiest ways to see this effect and is therefore one of the most widely studied. A thorough theoretical and experimental exploration of the penetration depth of the evanescent wave is given in a paper by Hall [1] and an experimental measurement of this phenomenon with electromagnetic waves was performed by Bose [2]. Later Culshaw and Jones [3] experimentally verified the predictions of Maxwell's equations for the transmission coefficient as a function of separation. This was later extended to account for the Goos-Hanchen shift by Renard [4]. A more in depth discussion of the background of this phenomenon can be found in Zhu *et. al.* [5].

In the coming sections we describe a mathematical model of the situation described above and test its validity against experimental data.

2 Theory

In Zhu *et. al.* [5] a theoretical derivation is given for plane waves in two semi-infinite media separated by a thin film of a third medium. The derivation starts from the Fresnel relations at both interfaces and accounts for infinitely many reflections by summing them in a geometric series. Then using the as-

sumptions of FTIR (angle of incidence ϕ is greater than the critical angle) they derive expressions for both the transverse electric (TE) and transverse magnetic (TM) modes for the coefficient of transmission due to evanescent waves during total internal reflection. For simplicity, we restrict ourselves only to the TM case and simplify the equations in Zhu *et. al.* by adding the assumptions that the index of refraction in the gap between prisms is 1 and that the two prisms have equal refractive indices. The equations are given below where R is the reflection coefficient, T is the transmission coefficient, n is the common index of refraction of the two prisms, ϕ is the angle of incidence of the incident waves (measured from normal), λ is the wavelength, and d is the perpendicular distance between the two prisms in meters.

From [5] we have

$$R = 1 - T$$
$$T = \frac{1}{\alpha \sinh^2 y + 1}$$

where

$$\alpha = \frac{((n^2-1)((n^2+1)\sin^2\phi - 1))^2}{4n^2\cos^2\phi(n^2\sin^2\phi - 1)}$$
$$y = \frac{2\pi d}{\lambda(n^2\sin^2\phi - 1)^{\frac{1}{2}}}$$

These equations assume the prisms are infinite, non-absorbing, and non-scattering. The waves are assumed to be planar and wholly contained within the infinite prisms. Built into the Fresnel relations that these are derived from is the assumption that all media are non-conducting, so that is also an assumption of these equations.

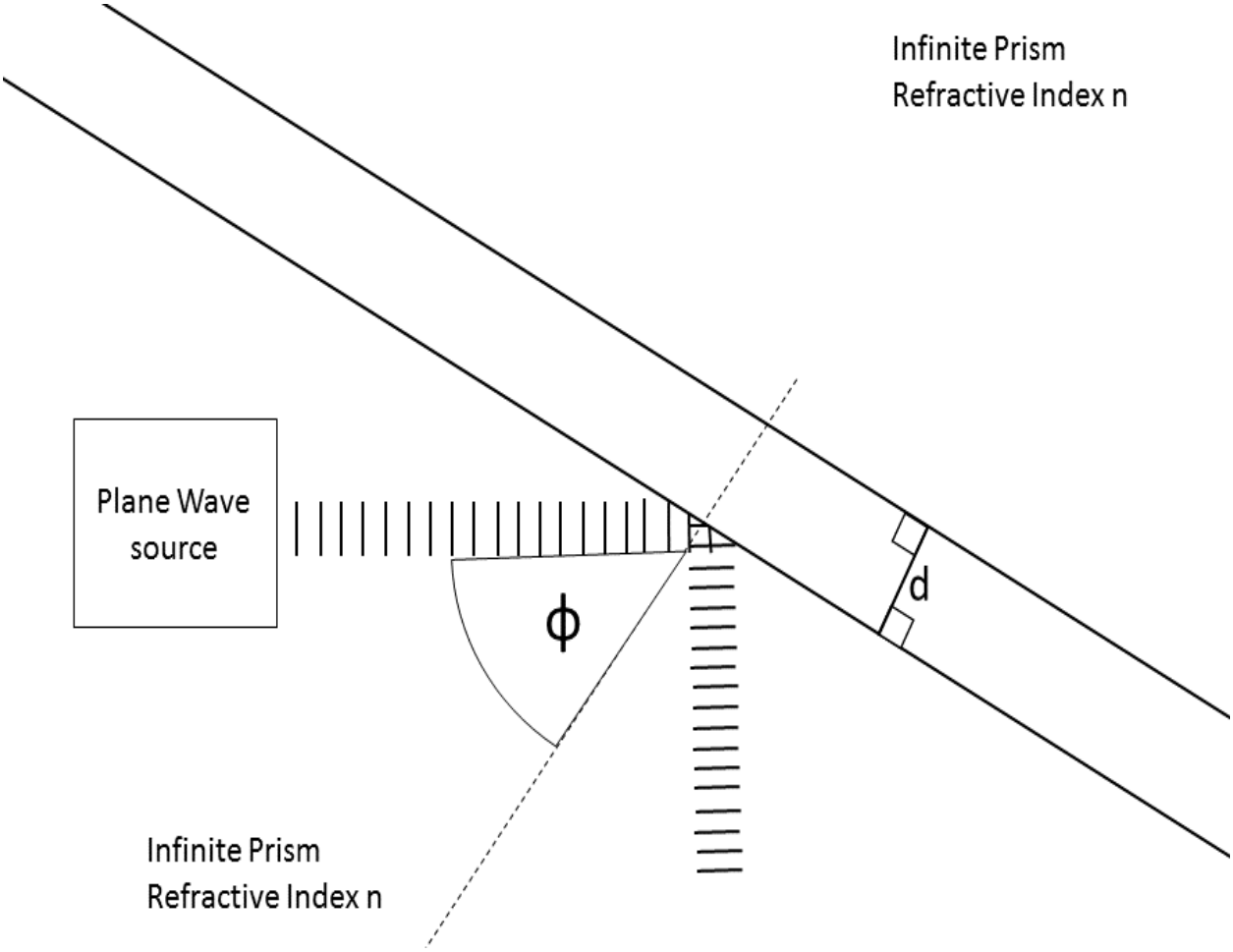

Figure 1: The setup used for theoretical derivation.

3 Methods

In order to make measurements to evaluate these theoretical predictions, the gap between prisms must be on the order of the wavelength. For these purposes we use two right triangle wax prisms made by cutting a single rectangular wax prism along one of its diagonals. This ensures that the refractive indices of the two prisms are as close as possible. The prisms are right triangular prisms with a long leg of 30 ± 0.1 cm, a sort leg of 17.9 ± 0.1 cm. As a source of waves we use a 15mW, 9 GHz microwave emitter with an attached horn antenna that produces a linearly polarized microwave such that the polarization is in the direction of one of the axes of the horn antenna. For field detectors we use two different emf probes. One is an Leybold emf probe mounted on a small rod with the measurement direction oriented along the axis of the rod and outputs an AC signal proportional to the square of the electric field. The second detector is a Pasco Scientific emf-probe with an attached horn antenna that measures electric field along one axis of the rectangular horn antenna and produces a DC voltage proportional to the square of the average magnitude of the electric field. Because the first emf probe outputs an AC signal we attach it to a lock in amplifier which samples the signal at the proper frequency and produces a voltage proportional to the maxima of the AC signal averaged over 10ms. So both probes produce a voltage proportional to the average value of the magnitude of the electric field squared.

In order to apply the theory given in the previous section, we had to determine a few properties of our system: the wavelength λ, the prism index of refraction n, and the angle of incidence ϕ. In the following sections we discuss how each of these quantities were experimentally measured. We then describe how the fields around the prisms were measured in order to give us some idea of how the fields reacted with the prism. Afterwards we explain how data measuring the transmission and reflection coefficients is done.

3.1 Measuring Wavelength

To measure the wavelength produced by our microwave transmitter we produced a standing wave and measured the magnitude profile. In order to produce a standing wave we placed the microwave transmitter so that the horn pointed directly towards an aluminum plate and the direction of travel for the wave was anti-parallel with the surface normal vector of the plate. We then changed the distance between the transmitter and plate until the magnitude of the standing wave anti-nodes was maximized. Using the rod mounted probe (as it is not directional) we moved the probe along the axis between the transmitter and plate taking data until a few full node/anti-node pairs had been found. This ensured that when we fit the data we would be fitting at least a few wavelengths.

3.2 Measuring Index of Refraction

To measure the index of refraction of the wax we tried many methods but the Michelson interfometer provided the smallest uncertainty. We setup a standard Michelson interferometer and placed the wax prisms so that their hypotenuses were flush and placed them in the beam path so that the beam entered and exited the prism normal to the surface of each side. With the prisms in this arrangement we then slid the prisms past one another to change the length of wax the interferometer beam had to propagate through. A diagram of the setup is shown in Figure 2.

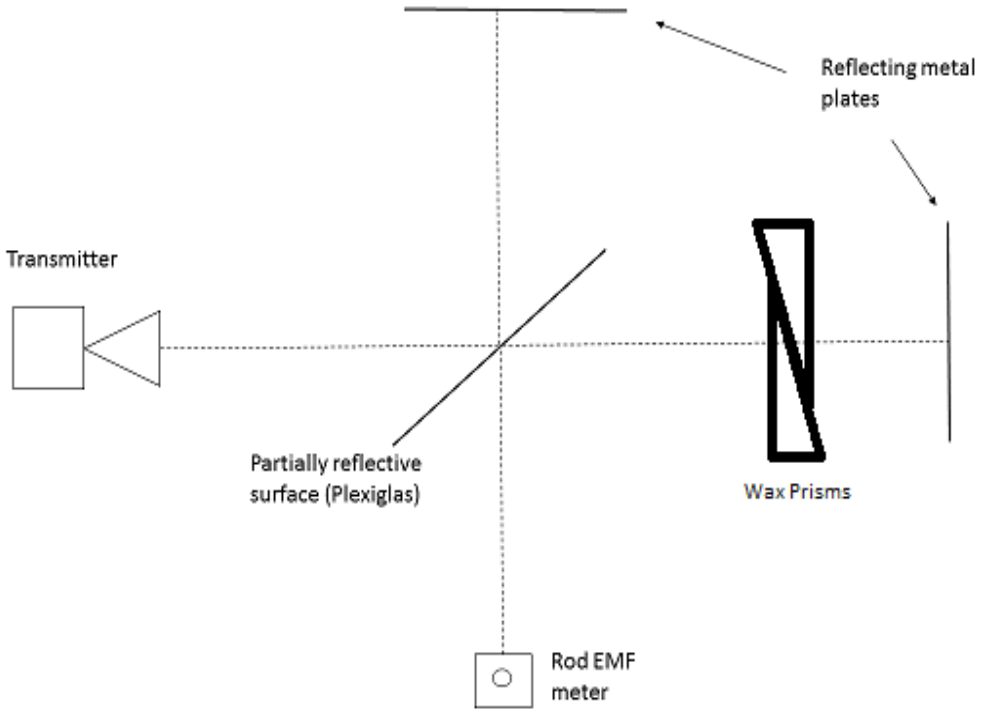

Figure 2: Michelson iterferometer used to measure the index of refraction of the wax prisms.

We starting the wax blocks with as little overlap of the hypotenuses as possible while also being confident that the beam was passing through the longer legs of each triangle. Then we took measurements of the electric field with the rod emf meter between which we increased the thickness of wax the beam was passing through. This was accomplished by pushing the wax blocks together enough so that their combined thickness increased about 1 cm between each reading.

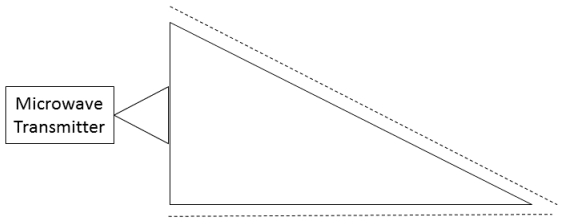

Figure 3: Measurement of edge fields around a single prism. Measurements were taken on the dotted lines.

3.3 Edge Fields

In order to see the effects caused by the edges of the prism interacting with the fields we measured the fields along each side. We first setup a single prism with the transmitter flush against the short side of the prism and measured the electric field in 1 cm increments along the other two sides (Figure 3). The rod detector was placed on the surface of the prism wherever the measurement was being taken. At each location 100 data points were taken over 10 seconds (at 10 Hz) and the average of these 100 were recorded as the data point with the standard deviation recorded as the uncertainty.

We then placed the second prism so that the hypotenuses were perfectly flush (0 cm separation) and took data along all available sides in the same way as described above (Figure 4). We then repeated the process after making a 1.1 cm air gap between the hypotenuses of the prisms. The measurements along the hypotenuse could obviously not be taken when the separation was 0 cm as there was no room for the detection rod. The 1.1 cm gap was chosen because it was the smallest possible gap in which our detector rod fit. The transmitter and detector were placed so that the beam reflected in the TE mode. We would have preferred to take measurements in the TM mode to match those done when measuring the transmission and reflection coefficients of FTIR but

the base of the rod detector was too large to allow us to place the detector horizontally in the gap between prisms and still have a separation of less then the wavelength. As a result we cannot be confident that any of these measurements are a realistic representation of the fields around the prisms during other parts of the experiment which were conducted in the TM mode.

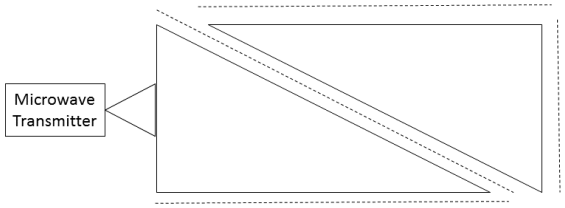

Figure 4: Measurement of edge fields around two prisms. Measurements were taken on the dotted lines.

3.4 Measuring Transmission and Reflection of FTIR

To measure the coefficients of reflection and transmission, one of the triangular wax prisms was mounted to a fixed point while the other was mounted on a drawer mechanism to smoothly roll and change the separation of the prisms. The transmitter was placed so that the opening of its horn antenna was flush to the short end of the fixed wax prism. The horn detector was placed so that its horn was open directly towards the opening of the transmitter horn and was flush with the short side of the mobile prism. The rod detector was placed on the long side of the fixed prism so that it detected the waves resulting from the reflection inside the first prism. An optical encoder was attached to the drawer mechanism with the output going to a microcontroller in order to keep track of the prism position.

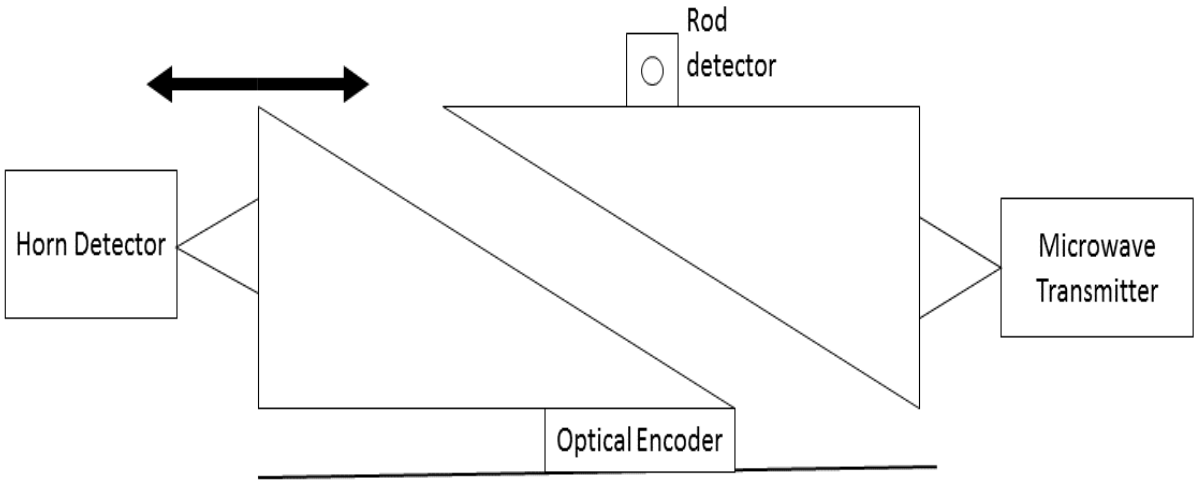

Figure 5: Setup for measuring the transmission and reflection coefficients of FTIR.

To obtain a data point the count of the optical encoder was reported and 100 values were read from each detector over 10 seconds (at 10 Hz). The 100 readings of each detector were then averaged and their standard deviation was taken. The average was recorded as the data point while the standard deviation was recorded as the uncertainty. The drawer was moved by hand to obtain prism separations of anywhere from 0 to 3.5 cm. We stop after 3.5 cm as this is definitely greater than the wavelength of our transmitter.

4 Results

Many of the raw results are given below in the same order that they were described in the Methods section. In the case of determining wavelength, a plot of the equation we fit it to is given as well.

4.1 Wavelength

The wavelength data appeared to fall off exponentially with distance from the transmitter, but it did oscillate periodically. Because of this we fit the data

to an equation of the form $Ae^{-ax} + B\sin^2(kx + b)$ as Ae^{-ax} is the general equation of a decaying exponential and something of the form $B\sin(kx + b)$ is the general form of a sinusoidal function. For our purposes the sine is squared to match the frequency doubling that occurs because we are measuring magnitudes on a standing wave. The precise form of the equation is not important though as we only needed to fit the data with some function with a sinusoidal component so we could find the wave number k. In order to determine the wavelength λ, we only had to fit the equation and notice that $k = \frac{2\pi}{\lambda}$. The fit was done using a least squares method with the 1 sigma uncertainties to determine a confidence interval for λ. The data is shown below in a plot. The x-axis of the plot contains only the values along a meter stick where measurements were taken and are not actually relative to anything as we only cared about the relative distance between waves. From the fit we calculate the wavelength from the fitted k to tell us $\lambda = 3.222 \pm 0.11$ cm.

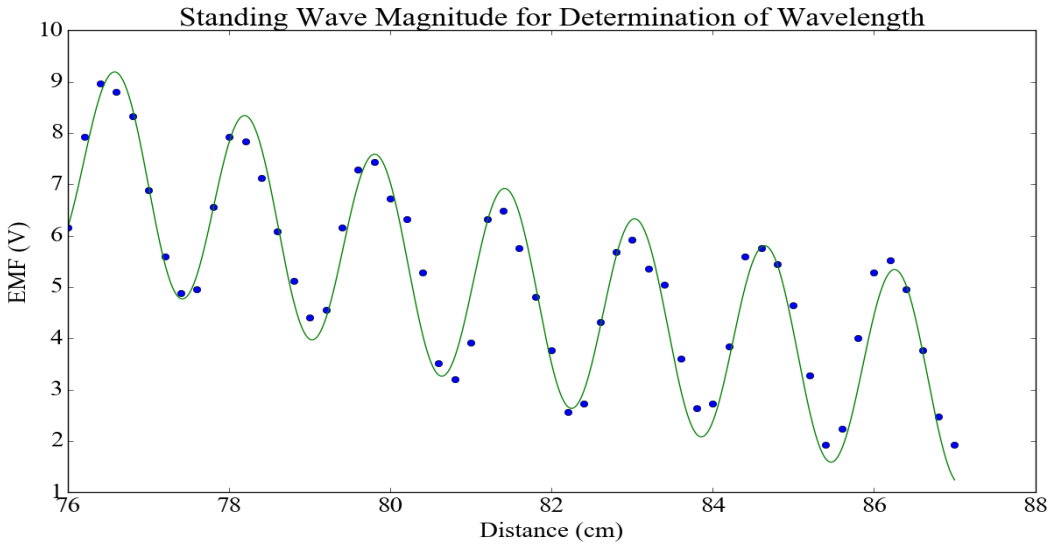

Figure 6: Magnitude of electric field standing wave over a distance along with a plot of the fit used to describe it.

4.2 Index of Refraction

Data from the Michelson interferometer to determine the wavelength is shown in Figure 7. Using the fact that it is a Michelson interferometer and considering the path difference we find $n = 1 + \frac{m\lambda}{2\delta x}$ where n is the index of refraction, λ is the wavelength determined in the previous section, and m is the number constructive/destructive interference cycles we complete in δx difference in distance. Using the λ calculated previously and estimating $m = 4 \pm 0.75$ cycles between 0.1 m and 0.237 m in the plot below, we get $n = 1.47 \pm 0.09$. Even with the large uncertainty of 0.75 in m this gives us a comparably small uncertainty in n and seems to agree with standard measures for chemically similar compounds like vegetable oils [6].

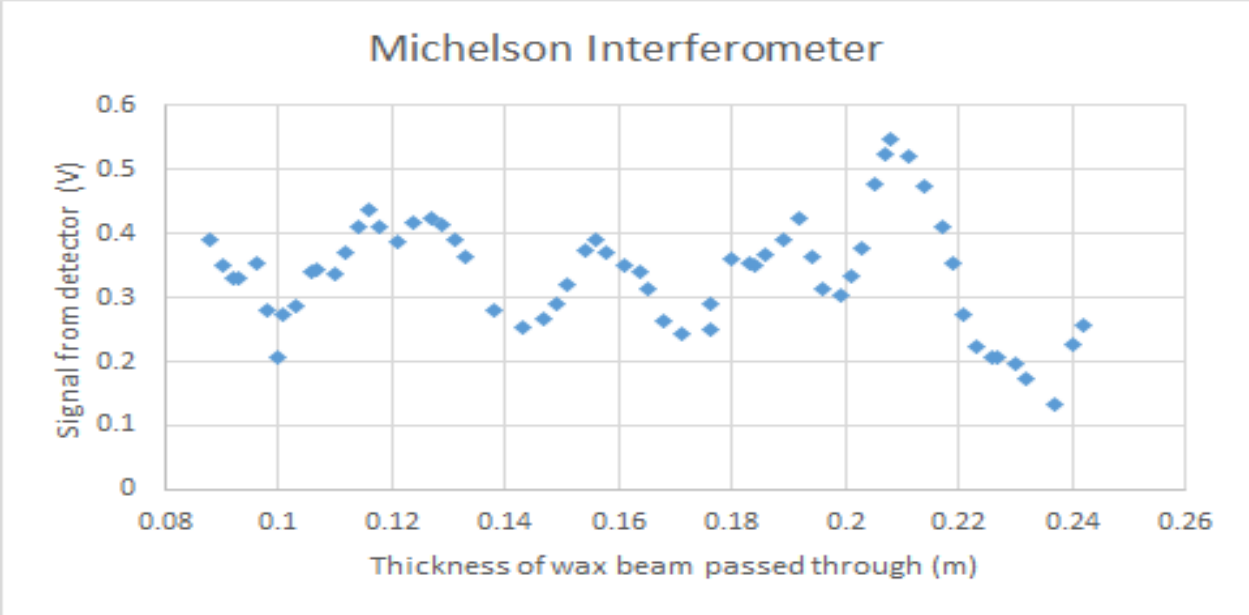

Figure 7: Magnitude of electric field in Michelson interferometer as a function of the thickness of wax on one arm of the interferometer.

4.3 Edge Fields

The data from each edge field measurement is plotted in **Apendix I**. Some interesting things to notice about these plots are that the electric field along the long side of a single prism (bottom side Fig. 3) and the exit face (right side Fig. 4) appear to have a pattern strikingly similar to interference patterns. These two figures are shown as figures 8 and 9. It is important to note again that all of these measurements were done in the TE mode and thus do not necessarily tell us anything about the rest of our experiment which is done in the TM mode.

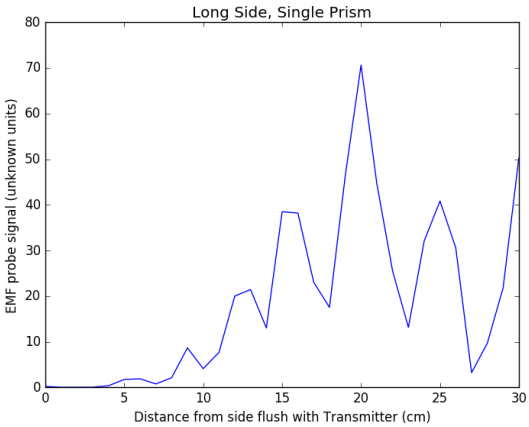

Figure 8: Electric field along side where reflecting beam emerges showing interference-like pattern.

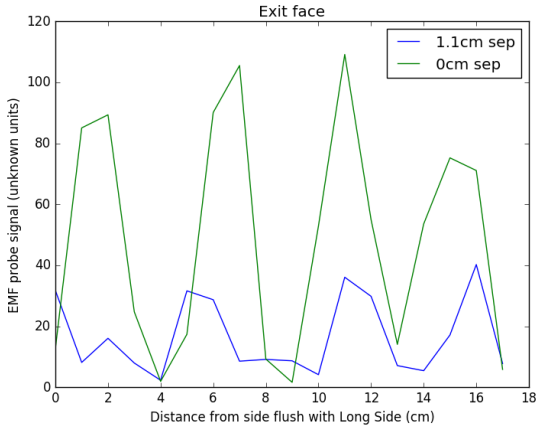

Figure 9: Transmission coefficient as a function of prism separation. One sigma uncertainty intervals are shown.

4.4 Transmission and Reflection Coefficients of FTIR

The transmission and reflection data were collected simultaneously in 5 separate trials. As you can see from the plots below though, the data was consistent within 1-sigma uncertainty for all 5 trials so the trials themselves are indistinguishable in the plots. You may also notice a small bare region around 0.6 cm separation where we were unable to take data. Anytime the drawer way placed in this region, it would quickly roll out as this region seemed like an unstable

equilibrium for the drawer.

According to the plot below, the transmission coefficient drops with increasing separation as we expect but it does not seem to level off at 0 cm like we would expect based on the equation for T given in the theory section.

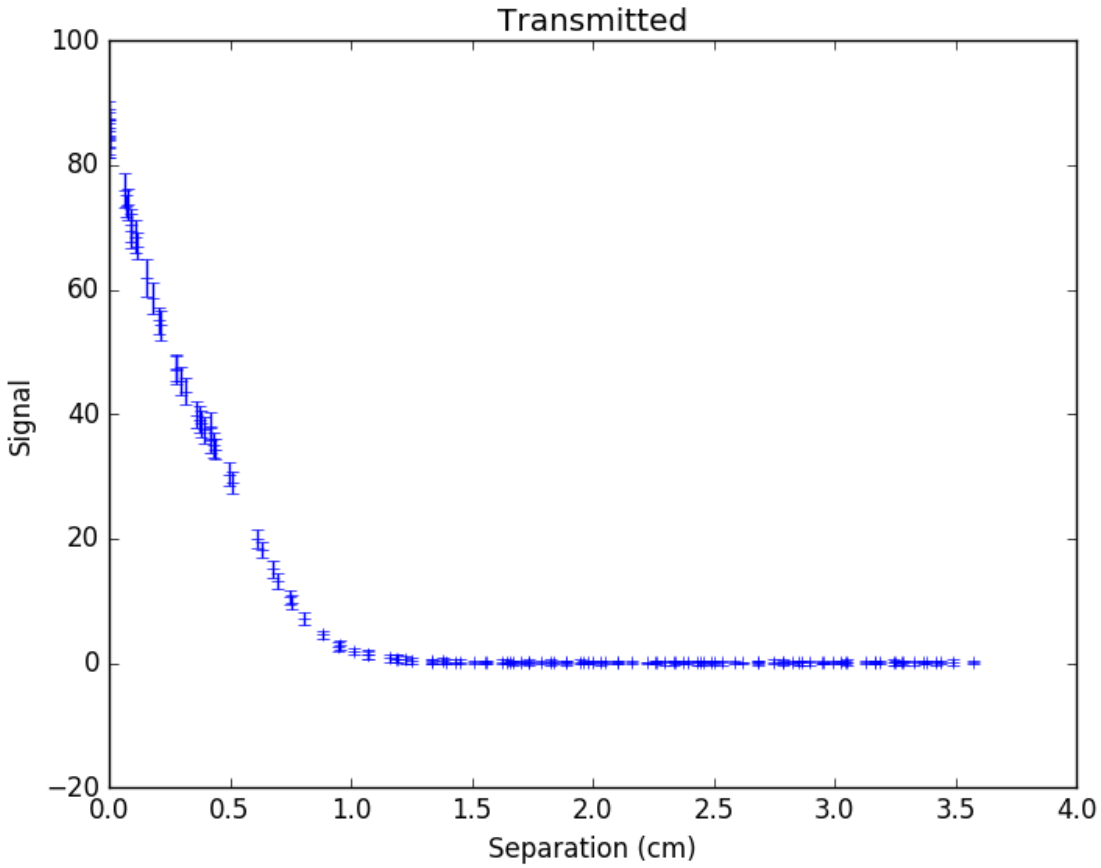

Figure 10: Magnitude of Transmitted wave in FTIR as a function of prism separation.

This reflection plot below is even more interesting. While the general trend is one that increases over time as we expect, there also appear to be large oscillations. These oscillations appeared in all 5 trials and are much larger than our uncertainty meaning that they are repeatable and they are not a product of noise in the data. Oscillations like this are not expected from the equation for R given in the Theory section so something else not accounted for in the theory must be effecting the results.

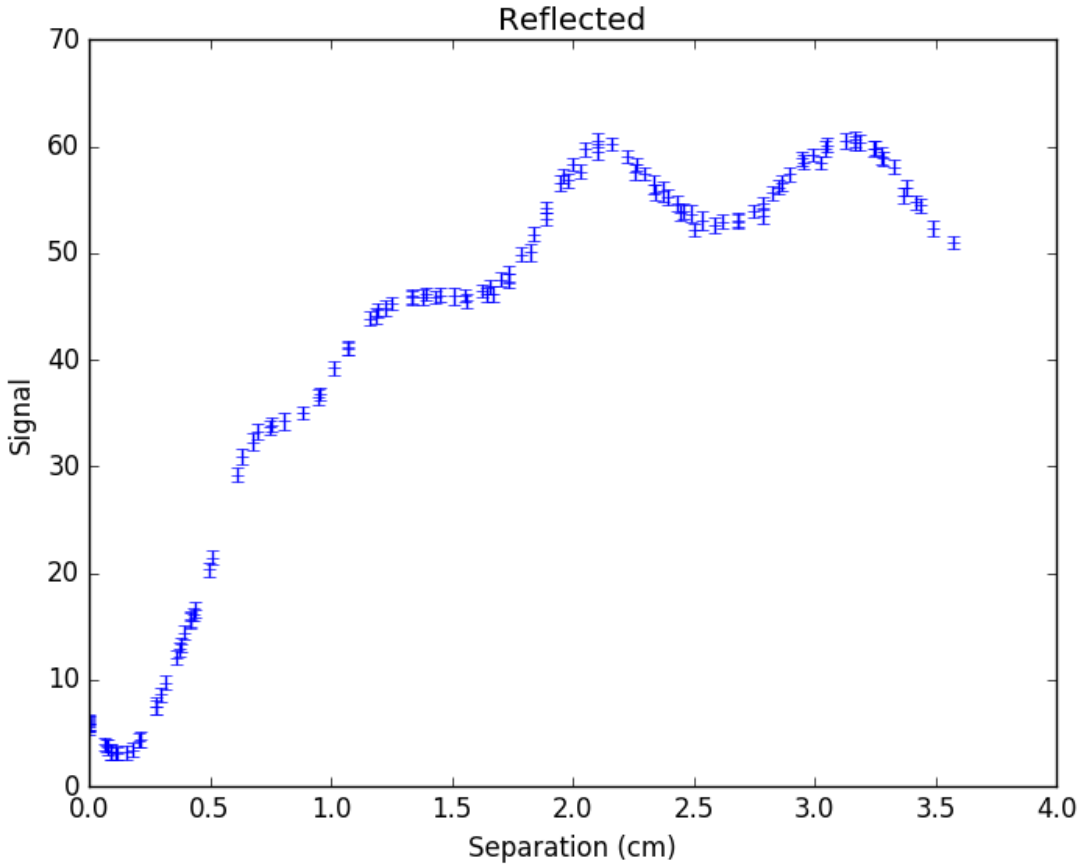

Figure 11: Magnitude of reflected wave in FTIR as a function of prism separation.

5 Conclusions

Since the reflected beam contains clear oscillations, it will obviously not fit the equation given in the theory section above. The oscillations also make the data extremely difficult to fit because based on the theory laid out by Zhu *et. al.* the reflective coefficient should rise asymptotically to a constant level, but this level would be hard to determine because of these oscillations. Because of this, we only attempt to fit the transmission coefficient data to theory.

With the experimental measurements we have taken for n, λ, and ϕ we can plug these into the equations given in the Theory section above to get a theoretical prediction for the transmission coefficient as a function of prism separation which is shown in yellow in the plot below. In order to find the normalization factor for the experimental data, a least squares fit was done between theory and the experimental data with a scale factor relating the two. The resulting normalized experimental data is shown in the plot below. The uncertainty intervals for both data sets are 1 sigma.

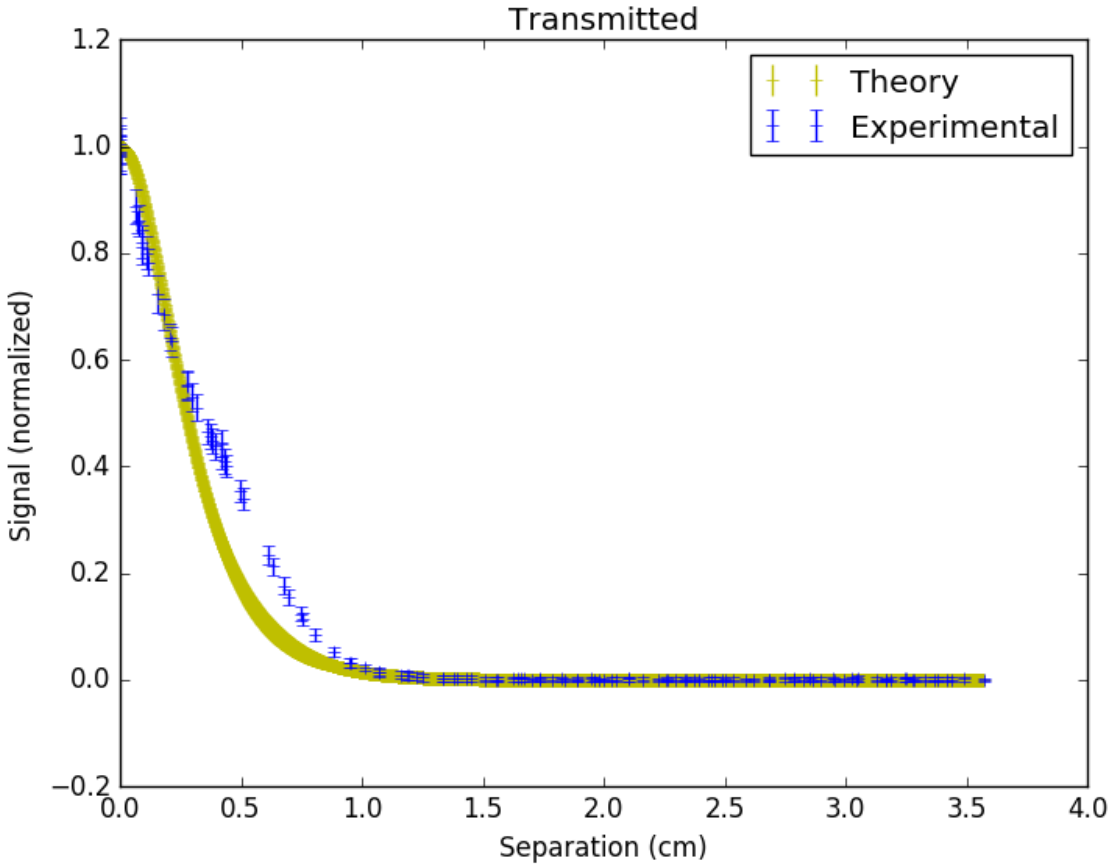

Figure 12: Transmission coefficient in FTIR as a function of prism separation, experimental and theoretical comparison.

As you can see, the two plots match well at large separations as they both tend to 0 while they only match in general trend for small separations. The experimental data almost appears to have some point around 0.4 cm separation where the data seems to level out slightly while the theoretical data is at its sharpest decline at that point. This could be caused by some extra oscillations in the transmission coefficient like those we saw in our reflected experimental data. We are unable to confirm whether these oscillations exist in this data set as any oscillations are smaller than the uncertainty and could thus be a product of a sampling anomaly. Overall, the most we can say about the agreement between experiment and theory is that they both follow the same general trend but obviously theory does not adequately predict what is occurring in this situation.

Because the data measuring the transmission coefficient were taken using the emf probe with an attached horn antenna which has a large opening and the field on the transmission edge was found to vary drastically from place to place (Fig. 9), we attempted to retake transmission data using the rod emf probe as it is more localized. Although we found the variations in the TE mode, there may be similar variations in the TM mode which we could find. We recorded data in the same way as we recorded the initial FTIR transmission measurements except that the horn probe was replaced with the rod probe. We then took measurements at the center of the face where the horn detector was previously centered (at ≈ 9 cm in Fig. 9) and off center at 7 cm in Fig. 9. The reason this was done was to compare the transmission signal received on and off the fringes in Fig. 9 as the horn of the horn detector is large enough for multiple fringes of the kind shown in Fig. 9 to enter the horn simultaneously. The transmission as a function of separation received at these two points is shown below with 1 sigma error bars.

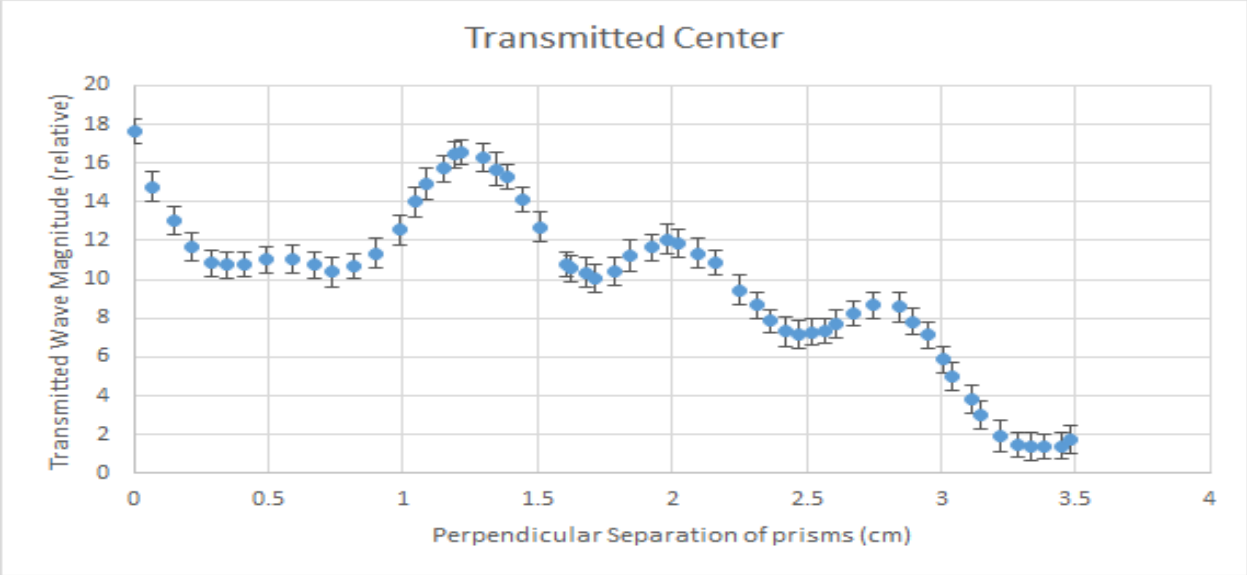

Figure 13: Transmission coefficient in FTIR as a function of prism separation, experimental and theoretical comparison.

In the plot of Figure 13 there are once again very clear oscillations. These oscillations are much larger than the uncertainty at these points and thus we know the oscillations are not a product of random sampling. Interestingly though, these oscillations have a different spacing between maxima than those found in the reflection coefficient data and so these oscillations must be caused by a different effect than what is creating oscillations in the reflection coefficient.

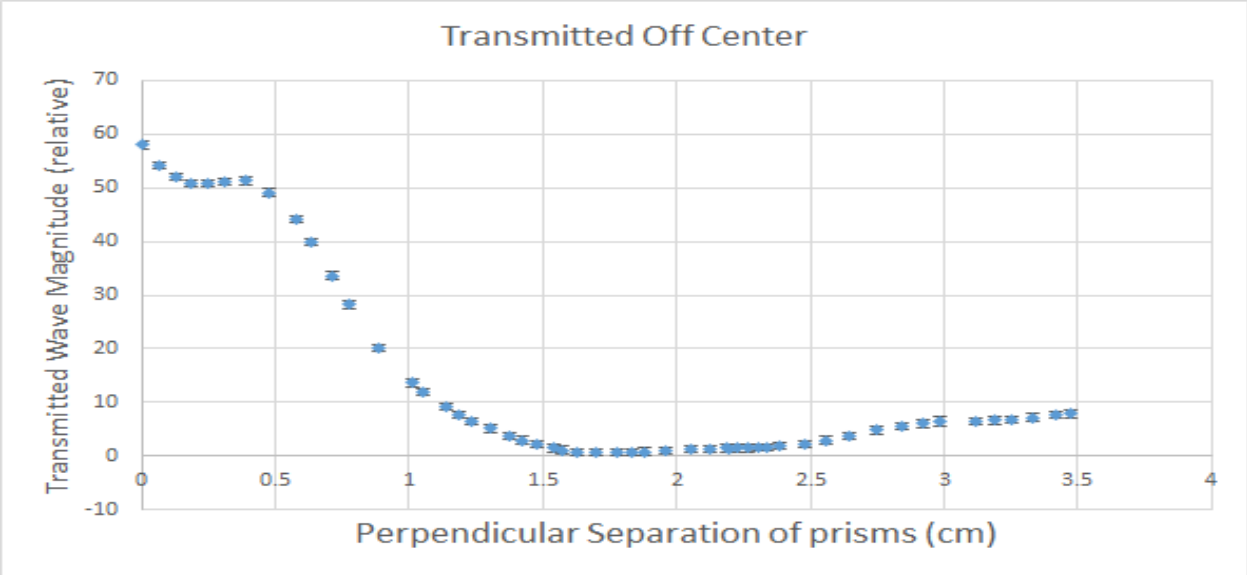

Figure 14: Transmission coefficient in FTIR as a function of prism separation, experimental and theoretical comparison.

The off center (on fringe) measurement shown in Figure 14 is much more of the shape we expect given the prediction from the Theory section. Other than very small and very large separations, this data seems to follow the trend quite well. After normalizing the experimental data so that the well shaped data at middle separations was closest to the corresponding theoretical values (using least squares), we get a plot comparing theory and experiment like the one shown in figure 15.

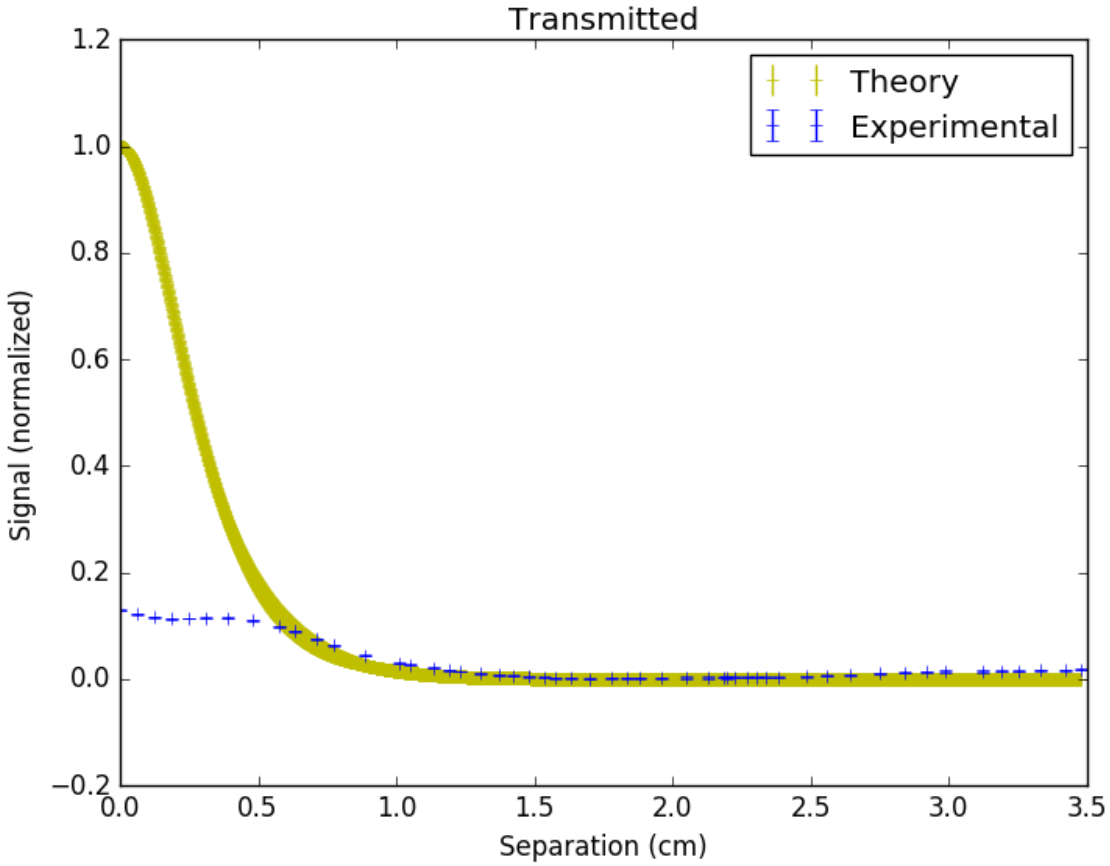

Figure 15: On fringe transmission coefficient in FTIR as a function of prism separation, experimental and theoretical comparison.

As you can see, the trends match most everywhere except low and high separations. Comparing the theoretical trend and the trend shown in the data, the major peak in our data appears to be severely cur off, but this could just be a product of how we fit the data. Assuming this fit is accurate this would mean that most of the waves that should be transmitted at low separations didn't make it through the prism. It is unknown precisely what could be causing this effect. If it were something like attenuation in the prism we would expect a similar drop in signal at all separations which would effectively be removed by normalization. This could be caused by something like beam walk off because the theory assumes the prisms are infinite which is not the case, but if that were the case we would expect a larger difference between theory and experiment at higher separations when the beams move further along the hypotenuse between each reflection.

If our work on this experiment showed anything it is that our microwave emitter does not produce a perfect beam of planar waves as the theory assumes. We believe many of the different oscillations found in our data are either caused by lobes of signal output by the horn antenna of our transmitter or from interference inside the prism caused because the beam diverges creating a wide variety of angles of incidence which then reflect and refract around inside the prism.

6 Future Work

In our work on this experiment there are obviously a few things that could have gone better. Here are some suggestions for future work.

1. Measure the edge fields and everything else in the same mode. Finding similar things for the edge fields in the TM mode would tell us that there actually are the fringes on the exiting face where transmission is measured.

2. Use an emitter that produces verifiably planar and colomated waves over at least a small area. This would help to avoid possible effects from the shape of the transmitter output and multiple paths due to divergence of the beam that may cause interference.

3. Use prisms much larger than the wavelength of your transmitter. Traditionally in optics, things can be approximated as infinite if they are much larger than the wavelength. In our case, the prism was only a few tens of wavelengths across at largest. This quite obviously does not satisfy the assumption made by the theory that the prisms can be treated as infinite.

4. Find a way to relate the reflected and transmitted data. Finding a way to relate these would enable us to know what the total beam getting reflected and transmitted was and may allow us to compensate for effects like attenuation of the beam inside the wax. The relation between the two data sets may also enable us to obtain more accurate data overall by giving us redundancy because then with just one of either the reflection or transmission data we would be able to predict what the other should be.

5. Another way of dealing with any of the problems addressed above would be to extend the theory to take into account things like the divergence of the beam, the prism being finite and producing interference from reflections inside the prism.

7 Acknowledgments

Every part of this research was performed in tandem with Andrew Baldrige so thanks alone does not give justice to his contribution. Thanks to Jacob Willig-Onwuachi for his technical insights in experimental setup and for his help in making sense of strange data. Thanks as well to Paul Tjossem who provided advice on experimental techniques and technological hurdles. Thanks to Grinnell College for providing laboratory space and equipment.

References

[1] E. E. Hall, Phys. Rev. 15, 73 (1902)

[2] J. C. Bose, Proc. R. Soc. London Ser. A 62, 300 (1897)

[3] W. Culshaw and D. S. Jones, Proc. Phys. Soc. B66, 859 (1953)

[4] R. Renard, Phys. Rev. 54, 1190 (1964)

[5] S. Zhu, A. W. Yu, D. Hawley, R. Roy, *Frustrated total internal reflection: a demonstration and review*, Am. J. Phys. 54, 601–606 (1986)

[6] "Refractive Index List of Common Household Liquids." International Gem Society. International Gem Society, n.d.

Apendix I

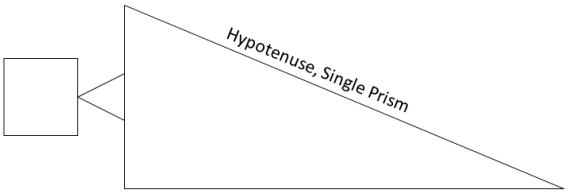

Long Side, Single Prism

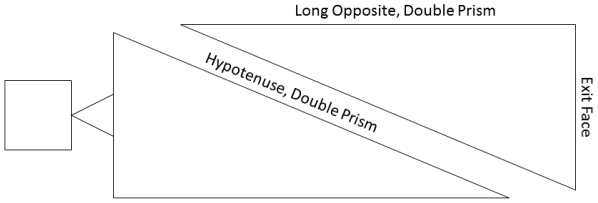

Long Side, Double Prism